Understanding Gel-to-Crystal Transitions in Supramolecular Gels

Demetra Giuri,[a] Libby J. Marshall,[b] Claire Wilson,[b] Annela Seddon,[c,d]* and Dave J. Adams[b,*]

a Dipartimento di Chimica Giacomo Ciamician, Alma Mater Studiorum, Università di Bologna, Via Selmi, 2, 40126, Bologna, Italy

b School of Chemistry, University of Glasgow, Glasgow, G12 8QQ, U.K.

c School of Physics, HH Wills Physics Laboratory, Tyndall Avenue, University of Bristol, Bristol, BS8 1TL, U.K.

d Bristol Centre for Functional Nanomaterials, HH Wills Physics Laboratory, Tyndall Avenue, University of Bristol, Bristol, BS8 1TL, U.K

Supporting Information

Experimental

Materials. The gelator 2NapAA was synthesized as previously described.[1]

Gelator Solutions. Stock solutions (20 mL) of 2NapAA (at a concentration of 5 mg/mL) were prepared by suspending the gelator (100 mg) in deionized water (17.10 mL). An equimolar ratio of NaOH (0.1 M, aq.; 2.90 mL) was added, and the solutions were gently stirred until a clear solution was formed.

The pH of the solution was checked and adjusted to 10.5 if needed using NaOH (0.1 M). To form gels, 2 mL aliquots of solution were placed in a 7 mL volume Sterilin vial containing a pre-weighed amount of glucono-δ-lactone (GdL). The samples were gently swirled to dissolve the GdL before being left to stand for 24 hours without stirring. After this time, the samples were examined by the vial inversion test to indicate gelation and any measurement was carried out at this point on a fresh sample for each measurement.

Rheology. All rheological measurements were performed using an Anton Paar Physica MCR101 rheometer. A vane and cup measuring system was used, setting a gap of 1.8 mm. The gels were prepared as described above and tested directly in the Sterilin cup which fits in the rheometer. Time Sweep experiments were performed at 25 °C using a constant angular frequency (ω) of 10 rad/s and a constant shear stress (γ) of 0.5%.

pH control. The pH of the gels was monitored with time after GdL addition, placing the Sterilin vials in a pre-equilibrated water bath to maintain a constant temperature of 25 °C. A FC200 pH probe (HANNA instruments) with a (6 mm x 10 mm) conical tip was employed for the pH measurements with a stated accuracy of ± 0.1. pH changes during the gelation process were recorded every 15 seconds for 16 hours.

To log the pH, a custom-built pH and temperature measurement and logging device was used. This is compatible with standard BNC-terminated pH probes and custom-built thermistor-based temperature probes and is capable of recording pH/temperature data over hours to days and then exporting these data as an ASCII file for further processing.
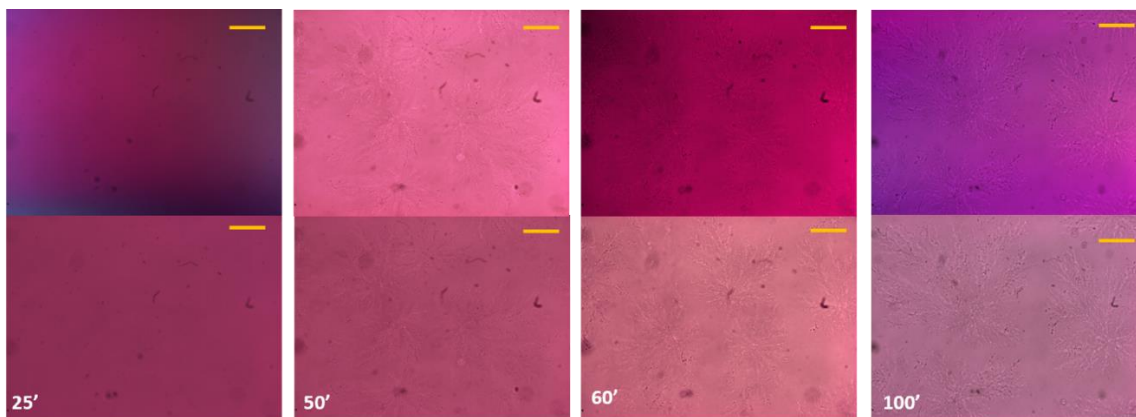
Optical Microscopy. All samples were prepared in a CELLstar®TC (Greiner Bio-One, Stonehouse, UK) 35/10 mm plastic cell culture dish. 1 mL of the gelator solution was mixed with the desired quantity of GdL, mixed to ensure dissolution of the GdL and placed in the dish. This was covered to prevent drying issues.

Confocal Microscopy. All samples were prepared in a CELLview™ (Greiner Bio-One, Stonehouse, UK) 35/10 mm plastic cell culture dish with a borosilicate glass bottom. Confocal microscope images were taken using a Zeiss LSM710 confocal microscope. Nile Blue was added as dye (2 μL of 0.1% w/w solution for every mL of gelator solution). 1 mL of the gelator solution was mixed with the desired quantity of GdL, mixed to ensure dissolution of the GdL and 0.4 mL of the solution placed in the dish. Fluorescence from Nile blue was excited using a 633 nm helium neon laser and emission was detected above 650 nm.

Single crystal X-ray diffraction. Single crystal x-ray diffraction data were collected using Bruker D8 Venture equipped with Photon II CPAD detector, dual IμS 3.0 Cu and Mo sources

Powder X-ray diffraction. PXRD (powder -ray diffraction) patterns were collected using a Rigaku MiniFlex 6G equipped with a D/teX Ultra detector, a 6-position (ASC-6) sample changer and Cu sealed tube (Kα1 and Kα2 wavelengths - 1.5406 and 1.5444 Å respectively). Patterns were measured as θ/2θ scans typically over a range of 3>2θ>60°. Data collection and analysis were carried out using Rigaku SmartLab Studio II software (Rigaku Corporation, 2014).

SAXS/WAXS. SAXS and WAXS data were collected on a Ganesha 300XL instrument (Xenocs). Samples were loaded into 3.5mm borosilicate glass capillaries (Capillary Tube Supplies Ltd) and sealed using optical adhesive (Norland) for 30 minutes under UV light. SAXS data were collected at room temperature over a Q range of $0.007 - 0.25\text{Å}^{-1}$ for an exposure time of 1800 seconds. WAXS data were collected at room temperature over a Q range of $0.07 - 2.8\text{Å}^{-1}$ for an exposure time of 600 seconds. All measurements were corrected for transmission and absolute intensity and had the water background and empty capillary scattering subtracted before processing. Data were reduced using SAXSGUI, and model fits were performed using SASView 4.0.4
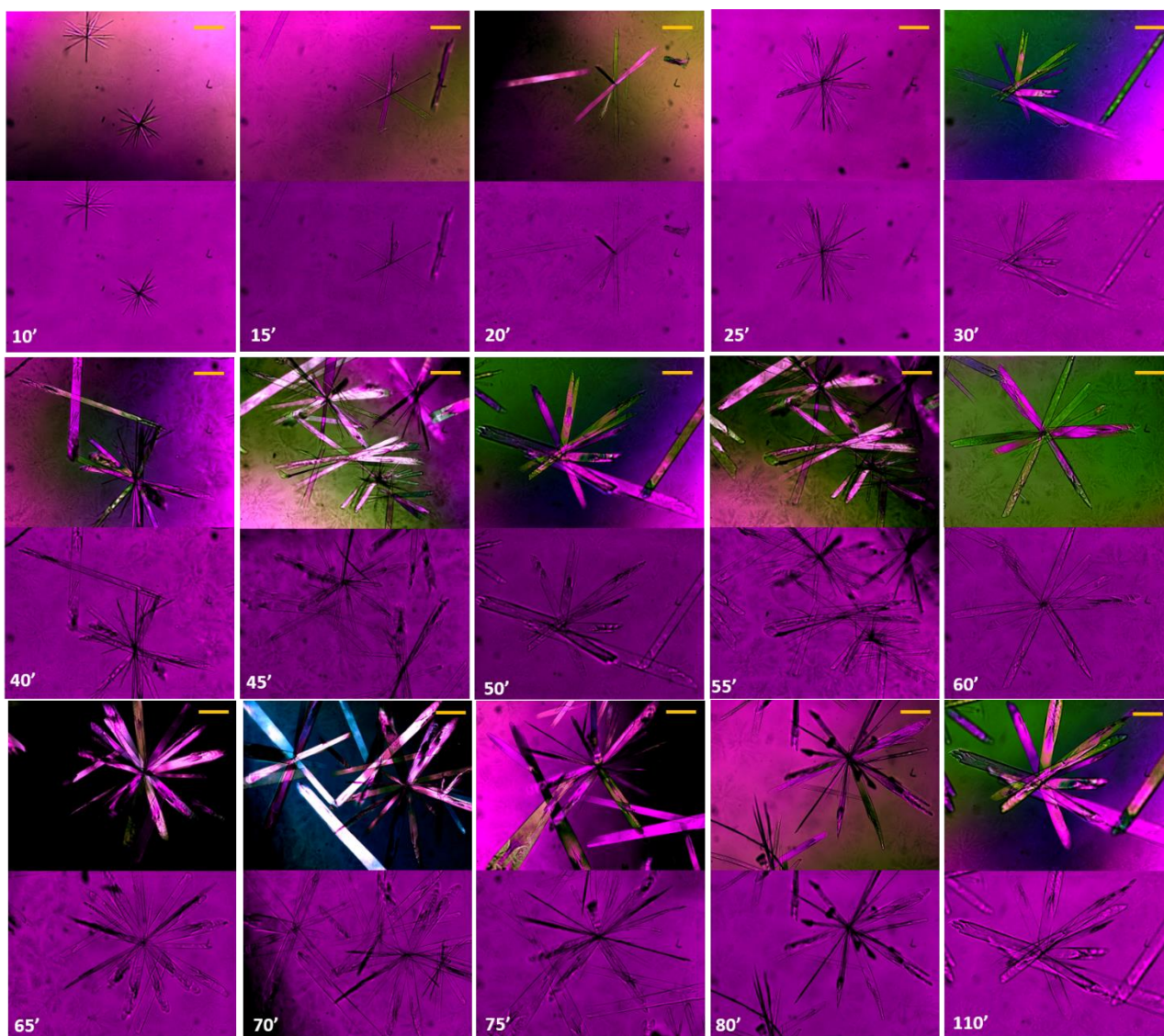

Figure S1. Optical microscope images (polarised light on the top) of sample **AA4** over time. The scale bar represents 300 µm**.** The colors are due to the use of plastic holders used to prepare the samples; all samples are transparent.
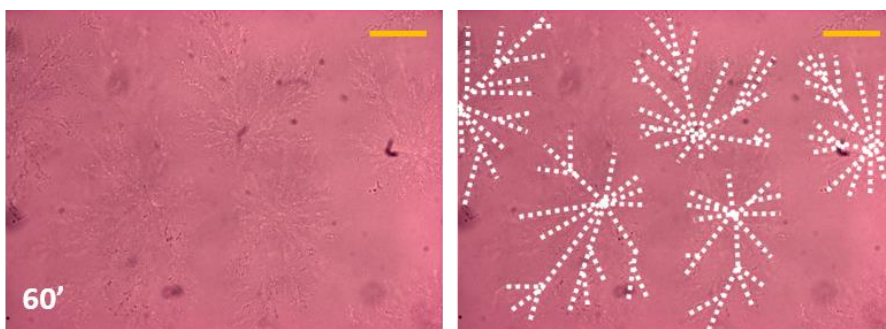
Figure S2. Comparison of optical microscope image for sample **AA4** at 60 minutes with an overlay showing where the spherulitic domains are for clarity. The colors are due to the use of plastic holders used to prepare the samples; all samples are transparent.
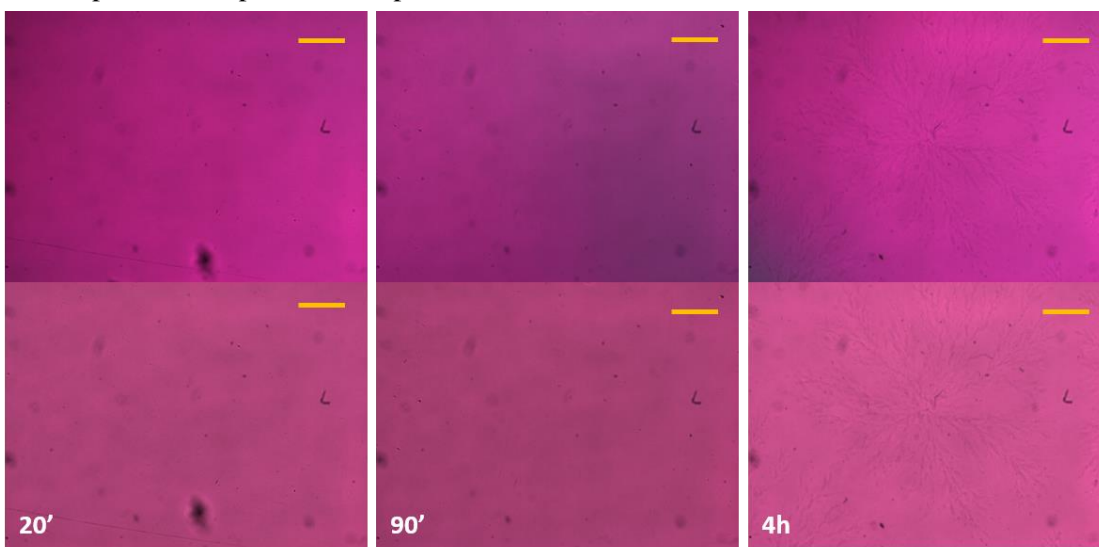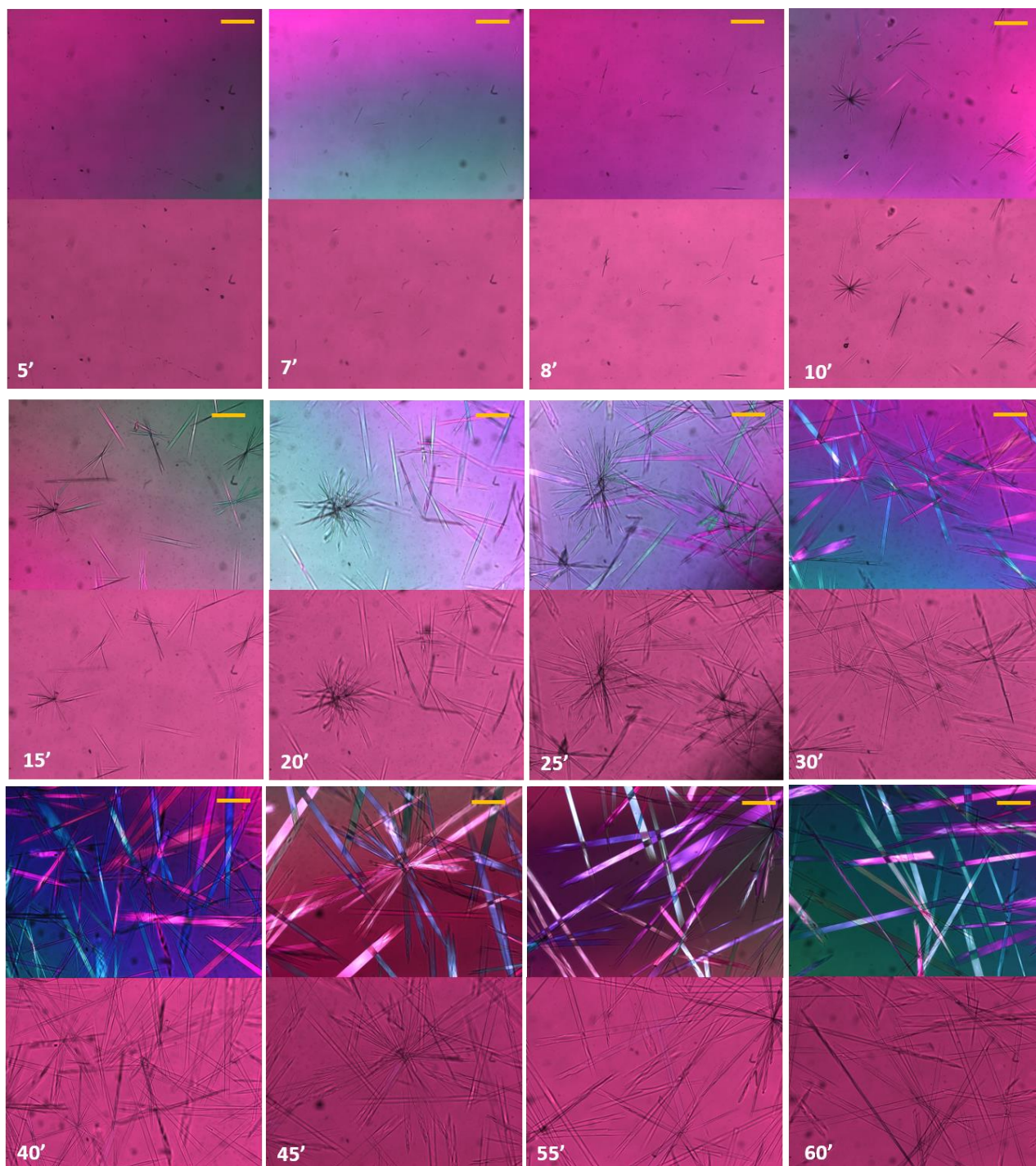

Figure S3. Optical microscope images (polarised light on the top) of sample **AA4(D)** over time. The scale bar represents 300 µm**.** The colors are due to the use of plastic holders used to prepare the samples; all samples are transparent.
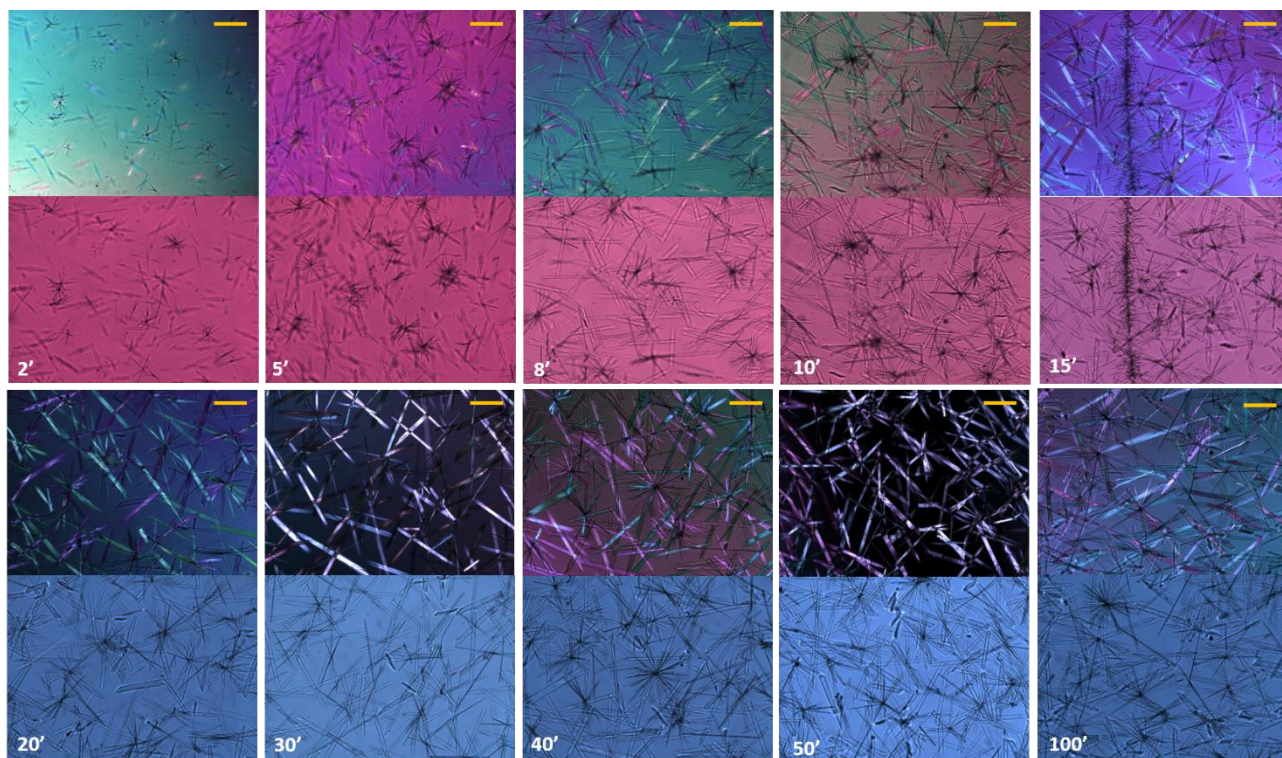
Figure S4. Optical microscope images (polarised light on the top) of sample **AA20** over time. The scale bar represents 300 µm. The colors are due to the use of plastic holders used to prepare the samples; all samples are transparent.

Figure S5. Optical microscope images (polarised light on the top) of sample **AA20(D)** over time. The scale bar represents 300 µm**.** The colors are due to the use of plastic holders used to prepare the samples; all samples are transparent.

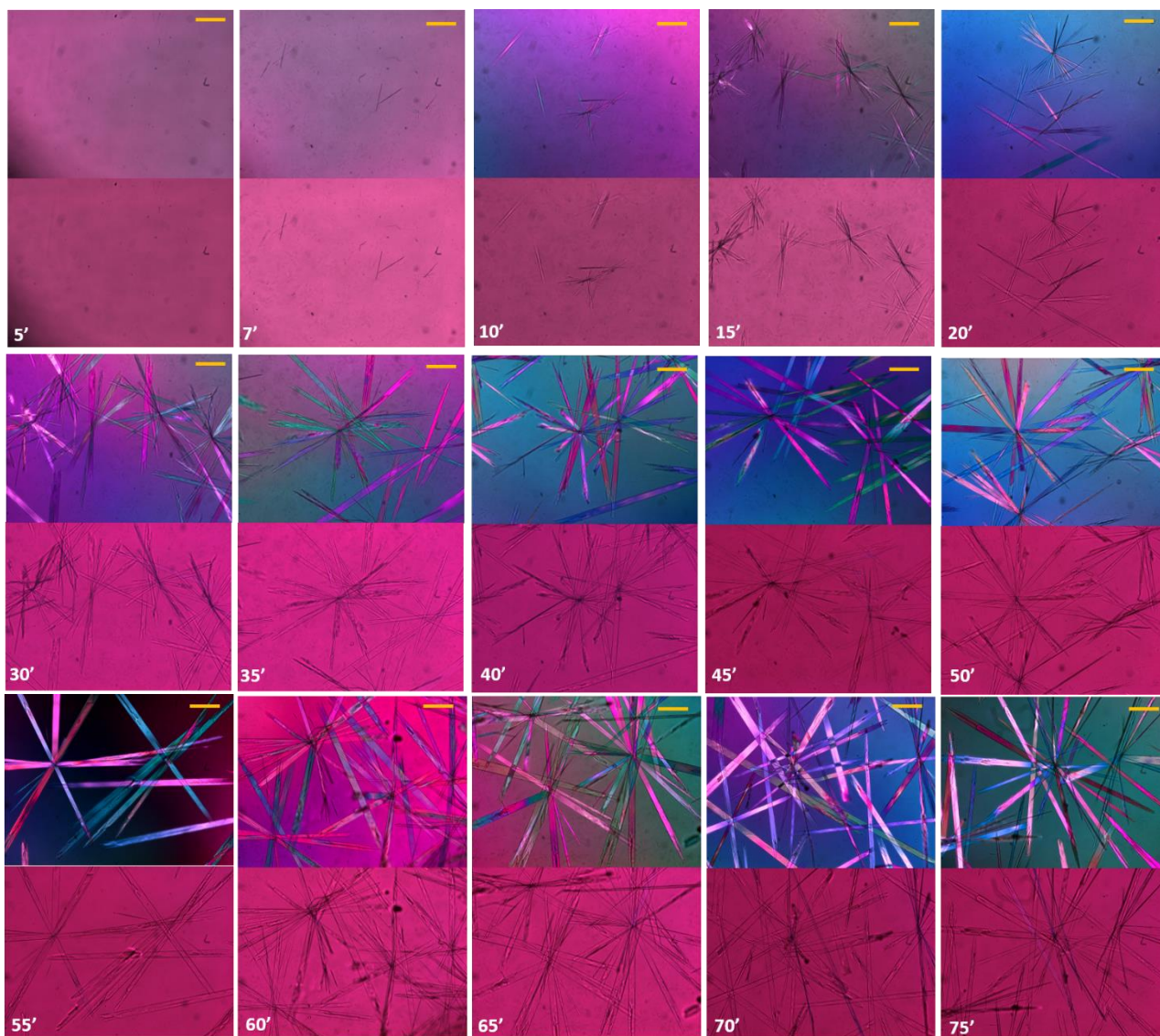**Figure S6.** Optical microscope images (polarised light on the top) of sample **AA36** over time. The scale bar represents 300 µm**.** The colors are due to the use of plastic holders used to prepare the samples; all samples are transparent.

Figure S7. Optical microscope images (polarised light on the top) of sample **AA36(D)** over time. The scale bar represents 300 µm**.** The colors are due to the use of plastic holders used to prepare the samples; all samples are transparent.

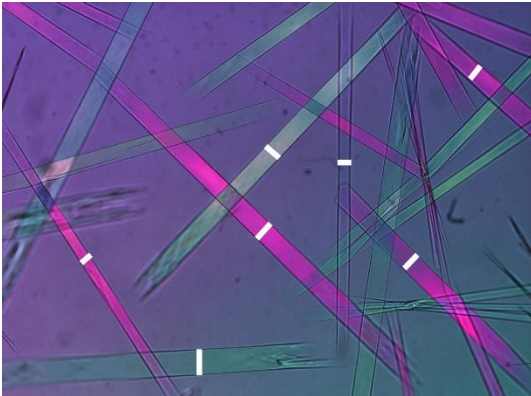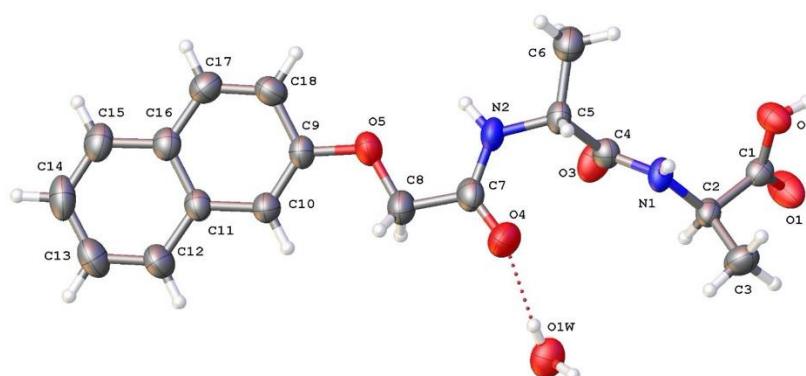| AA20			
Time	n	Mean (μm)	SD (μm)
20'	25	41,98	15,67
45'	40	71,52	21,85
60'	40	70,65	25,41
AA20(D)			
Time	n	Mean (μm)	SD (μm)
20'	25	40,10	11,19
45'	40	46,57	16,36
60'	40	45,92	19,45

Table S1. Crystal dimension measurements. The cross-section of the crystals for samples **AA20** and **AA20(D)** were measured from optical microscope images using the freely distributed software Gimp 2.8 (GNU Image Manipulation Program). The mean diameter was evaluated from optical microscope photos at different times (20', 45', 60'), randomly gathering the crystals. For 20' images, 25 diameters were collected since fewer crystals were present in the sample, while for 45' and 60' it was possible to collect 40 measurements. An example image is shown – the measured cross-sections are shown as white lines on the crystals.

Room temperature single crystal structure

The structure was determined from diffraction data collected at room temperature to facilitate comparison with the pXRD data. The structure is essentially the same as that reported from data measured at 100K.[3]

Crystal data. $C_{18}H_{20}N_2O_5 \cdot H_2O$, M = 362.37, orthorhombic, a = 5.8565 (7), b= 8.6565 (12), c = 36.543 (6) Å, U = 1852.6 (4) Å^3, T = 295 K, space group $P2_12_12_1$ (no.19), Z = 4, 8786 reflections measured, 3499 unique (Rint = 0.051), which were used in all calculations. The final w$R(F^2)$ was 0.099 (all data). Crystallographic data for CCDC2053987 are available free of charge from The Cambridge Crystallographic Data Centre (https://www.ccdc.cam.ac.uk). The structure was determined from diffraction data collected at room temperature to facilitate comparison with the pXRD data. The structure is essentially the same as that reported from data measured at 100K (CCDC refcode NUVHIX).[1,3]


Figure S8. Crystal structure of 2NapAA grown directly from the gel phase in H_2O. Atomic displacement ellipsoids drawn at 50% probability level.

Powder x-ray diffraction

Powder x-ray diffraction patterns were measured for the samples **AA20**, **AA36**, **AA4(D)**, **AA20(D)** and **AA36(D)** and are shown in Figures S9 (for H_2O) and S10 (D_2O) with the pattern calculated from the room temperature single crystal structure of 2NapAA
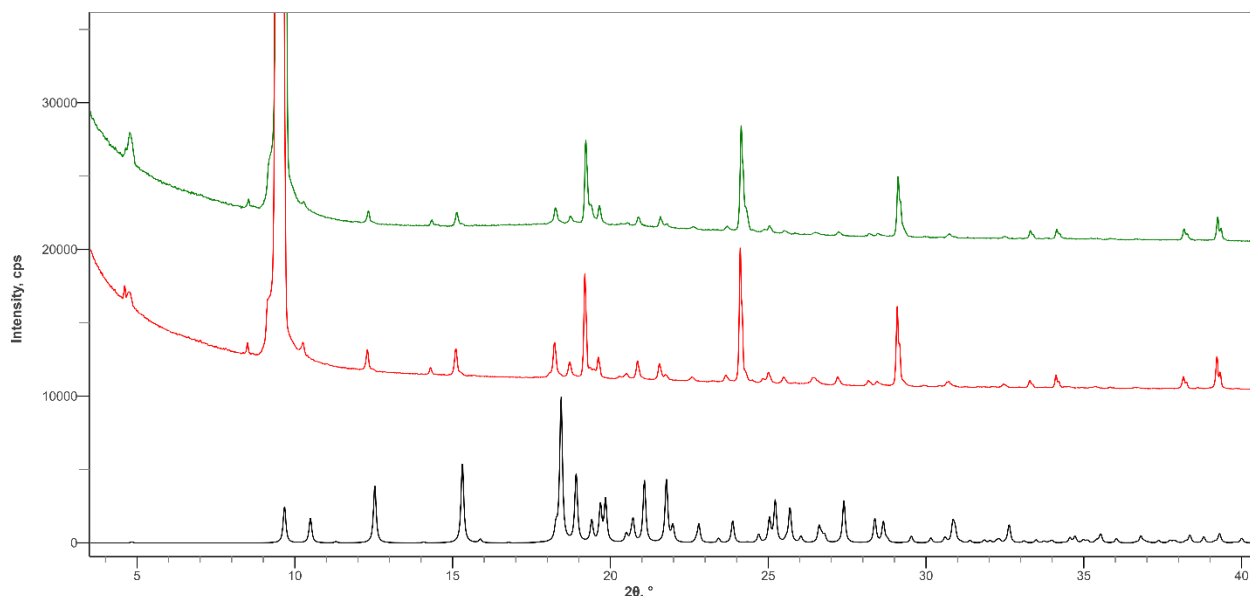
Figure S9. pXRD patterns for **AA20** (red) and **AA36** (green) with calculated pattern from the room temperature crystal structure shown in black.
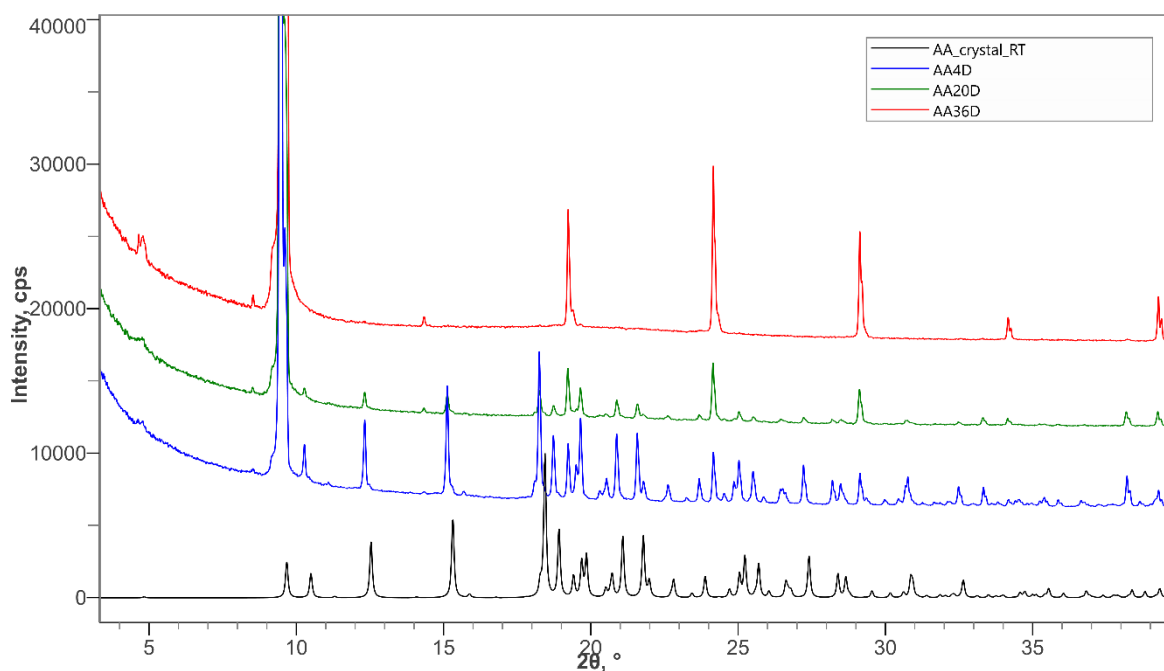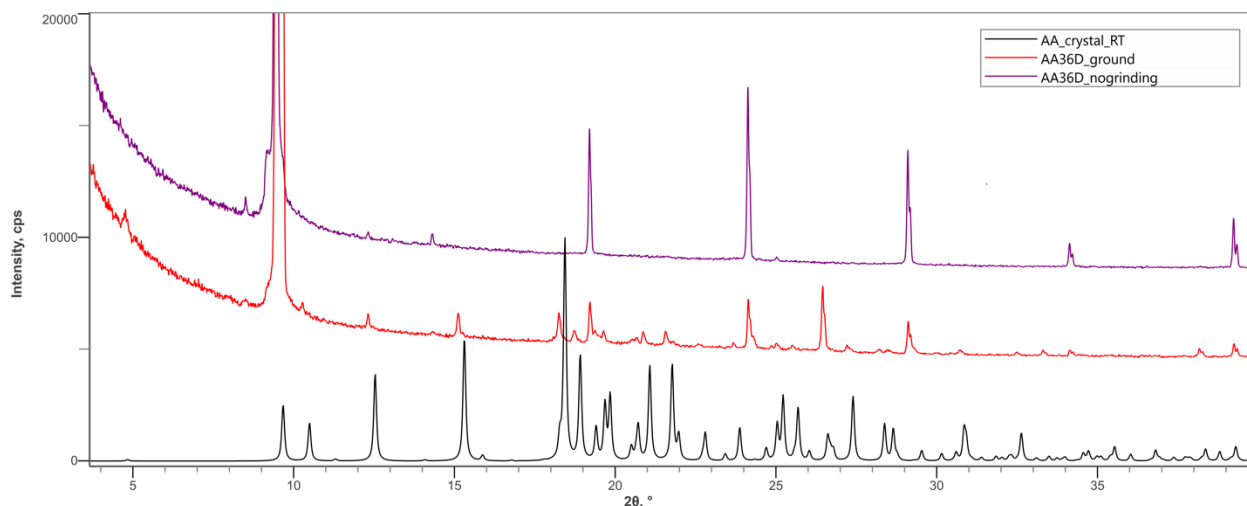

Figure S10. pXRD patterns for **AA4(D)** (blue), **AA20(D)** (green) and **AA36(D)** (red) with calculated pattern from the room temperature crystal structure shown in black.

All samples are the same crystalline phase and match the room temperature structure of 2NapAA. On first examination it is not clear that these do in fact all match, particularly those for **AA36** and **AA36D** and for other samples the relative peak intensities are not a good match. However, this is due to a strong preferred orientation

effect. The crystallites formed are all very anisotropic in shape, crystallising as long thin columns, which reflect the unit cell dimensions are a = 5.8565 (7), b= 8.6565 (12), c = 36.543 (6) Å. The higher quantities of GdL decrease the pH more rapidly resulting in quicker growth and more anisotropic crystals which is reflected in the increased preferred orientation effects. The effect is due to the preferred orientation of the crystallites where long rod-shaped crystallites align rather than having all orientations present. This leads to relative intensity of the 00l reflections being greatly enhanced in this case (2θ positions of selected reflections are given in Table S2). In **AA36** and **AA36D** the effect is so strong an effect that the 002n reflections appear to the exclusion of almost all others. In the initial measurements we were keen to measure the patterns with minimal handling of the sample. However, to show that the samples are NapAA we measured a pattern for AA36D before and after grinding the crystals, to reduce this alignment of crystallites, and the results are shown in Figure S11, and the match is much improved.


Figure S11. pXRD patterns for **AA36** with no grinding (purple) and with grinding (red with calculated pattern from the room temperature crystal structure shown in black showing the effect of preferred orientation in the non-ground samples.

2θ (°)	h k l	Inorm	2q (°)	h k l	Inorm
4.83	0 0 2	0.75	18.44	1 1 1	100
9.67	0 0 4	24.95	19.42	0 0 8	0.30
10.49	0 1 1	17.20	24.34	0 0 10	0.46
12.53	0 1 3	38.70	29.30	0 0 12	0.30
14.08	0 1 4	0.53	34.33	0 0 14	0.07
14.53	0 0 6	0	39.42	0 0 16	0.09
15.31	1 0 1	55.79			

Table S2. 2θ values for the selected reflections (hkl) and the Inorm value gives the calculated relative intensity scaled to 100% for the strongest peak.

Time / min	150	180	210	270	300	330
Model	Flexible cylinder	Flexible cylinder	Flexible cylinder	Flexible cylinder	Flexible cylinder	Flexible cylinder
Scale	$3.9 \times 10^{-5} \pm 1.6 \times 10^{-5}$	$4.6 \times 10^{-5} \pm 1.5 \times 10^{-5}$	$6.2 \times 10^{-5} \pm 2.3 \times 10^{-6}$	$8.0ex10^{-5} \pm 3.2 \times 10^{-6}$	$0.0003 \pm 9.0 \times 10^{-6}$	$9.5 \times 10^{-5} \pm 2.91 \times 10^{-6}$
Background	0.005 ± 0.0002	0.006 ± 0.0002	0.005 ± 0.0002	0.006 ± 0.0002	0.005 ± 0.0002	0.005 ± 0.0002
Length / Å	>1000	>1000	>1000	>1000	>1000	>1000
Kuhn length / Å	48.4 ± 25.0	54.7 ± 16.9	159.2 ± 16.9	190.3 ± 10.8	204.9 ± 12.8	209.2 ± 12.2
Radius / Å	29.2 ± 1.4	29.7 ± 2.6	39.5 ± 1.2	41.9 ± 1.1	40.9 ± 1.0	41.2 ± 0.90
Chi^2	1.54	1.64	1.98	2.07	1.88	2.89

Table S3. SAXS Model fitting parameters for low concentrations of GdL leading to gelation of 2NapAA. Note that no fittable data was obtained at time points below 150 minutes.
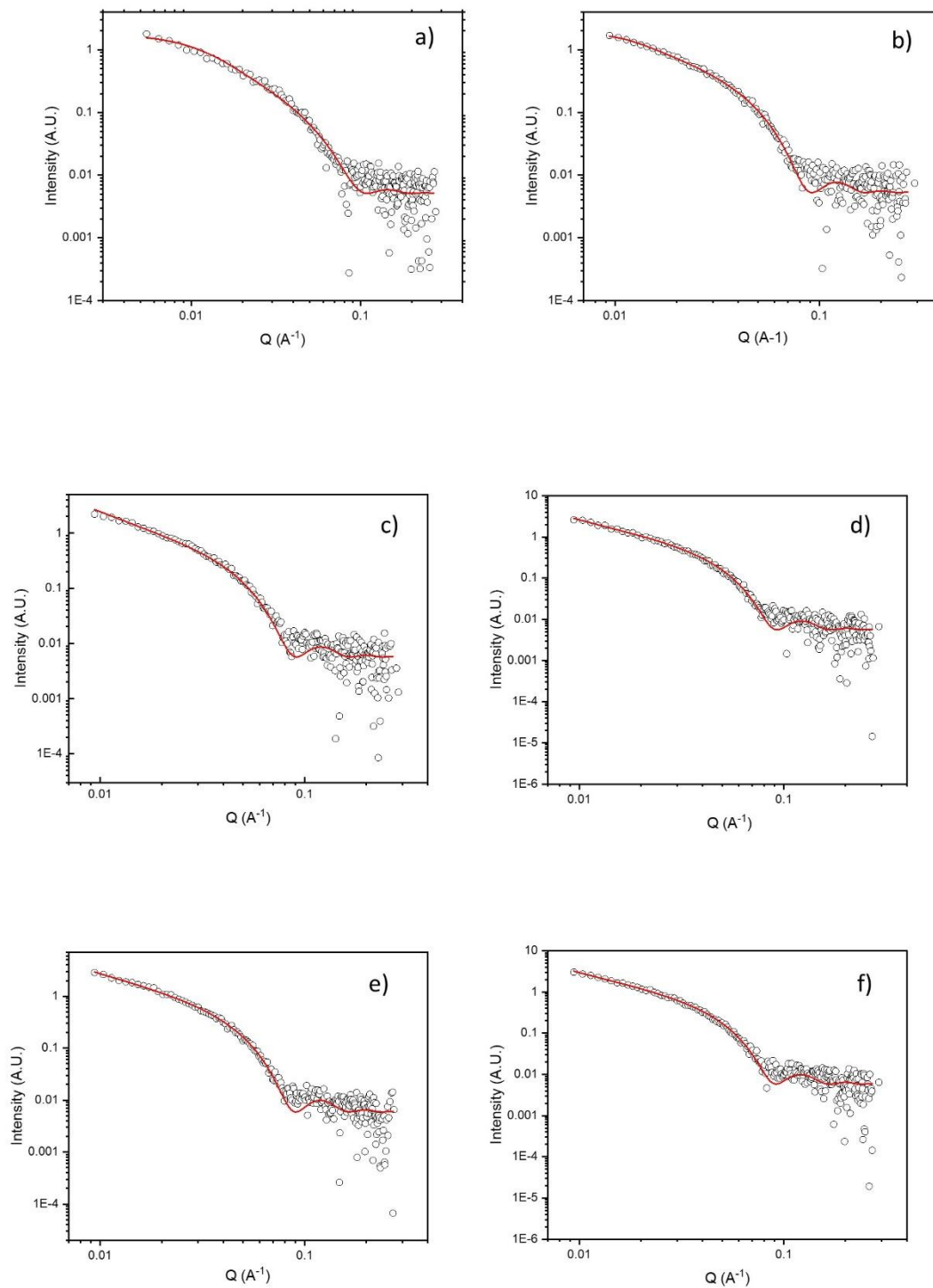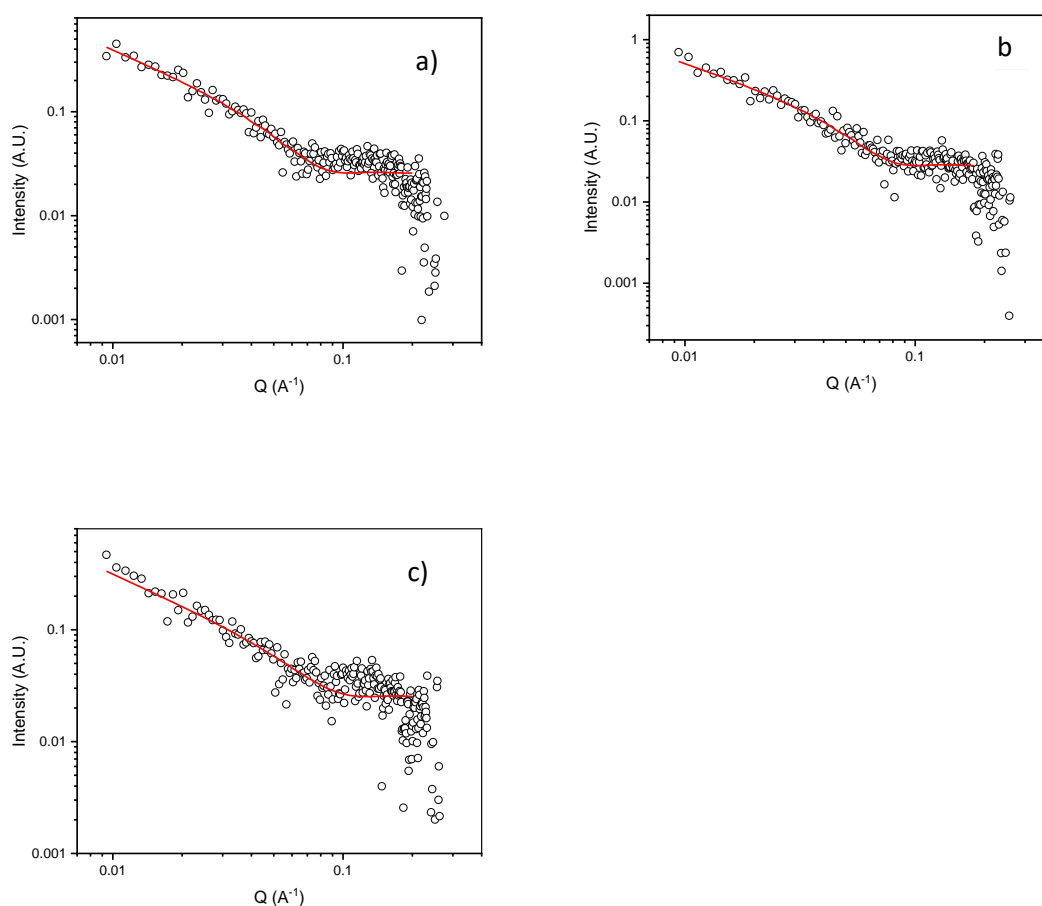
Figure S12. SAXS data showing gelation with time (black circles) with overlaid form factor fit to a flexible cylinder model (red line): a) 150 min; b) 180 min; c) 210 min; d) 270 min; e) 300 min; f) 330 min

| Time / min	60	100	140
Model	cylinder	cylinder	cylinder
scale	$0.0001\pm6.4\times10^{-6}$	$0.0004\pm2.1\times10^{-5}$	$0.0004\pm3.1\times10^{-5}$
background	0.03 ± 0.0005	0.03 ± 0.0006	0.03 ± 0.0006
length	>1000	>1000	>1000
radius	36.0 ± 1.5	37.9 ± 1.3	30.2 ± 1.5
Chi^2	2.56	1.98	2.72

Table S4. Form factor fitting parameters obtained for SAXS patterns taken during the first three measurements of gelation of 2NapAA. Note that the smaller radius seen for the measurement at 140 minutes is likely due to the breakdown of the gel and onset of crystallisation that occurs during this time period, as evidenced by the corresponding WAXS data.


Figure S13. SAXS data showing gelation with time (black circles) with overlaid form factor fit to a flexible cylinder model (red line) for higher GdL concentration, prior to crystalisation: a) 60 min; b) 100 min; c) 140 min.

| WAXS peak position (2θ / °)	pXRD peak position (2θ / °)	Calculated d from PXRD (Å)	plane
9.42	9.67	9.136	004
12.6	12.53	7.056	013
15.44	15.31	5.78	101
18.63	18.50	4.8	111
19.4	19.41	4.5	105
27.96	27.40	3.25	124
30.67	30.61	2.919	1110

Table S5. Comparison of peaks between the collected WAXS data and the simulated PXRD pattern for 2NapAA showing the corresponding d value and the assigned plane.
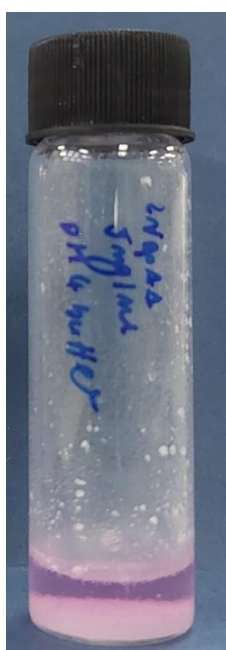
Figure S14: Photograph of 2NapAA directly suspended in pH 4 buffer, showing that the gelator is insoluble under direct suspension at low pH. No gel formation is observed.
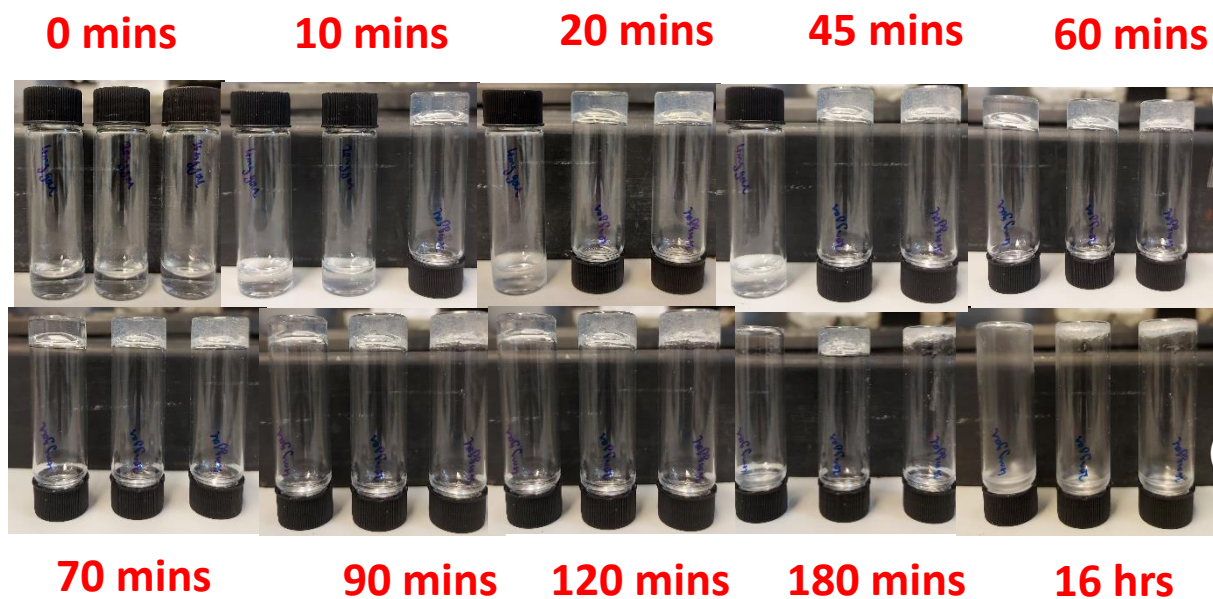
Figure S15: Photographs showing the effects of reduced temperature on gelation rates. Left to right for each time point samples are a 5mgL-1 solution of 2NapAA with 4mg GdL, 20mg GdL and 36mg GdL.
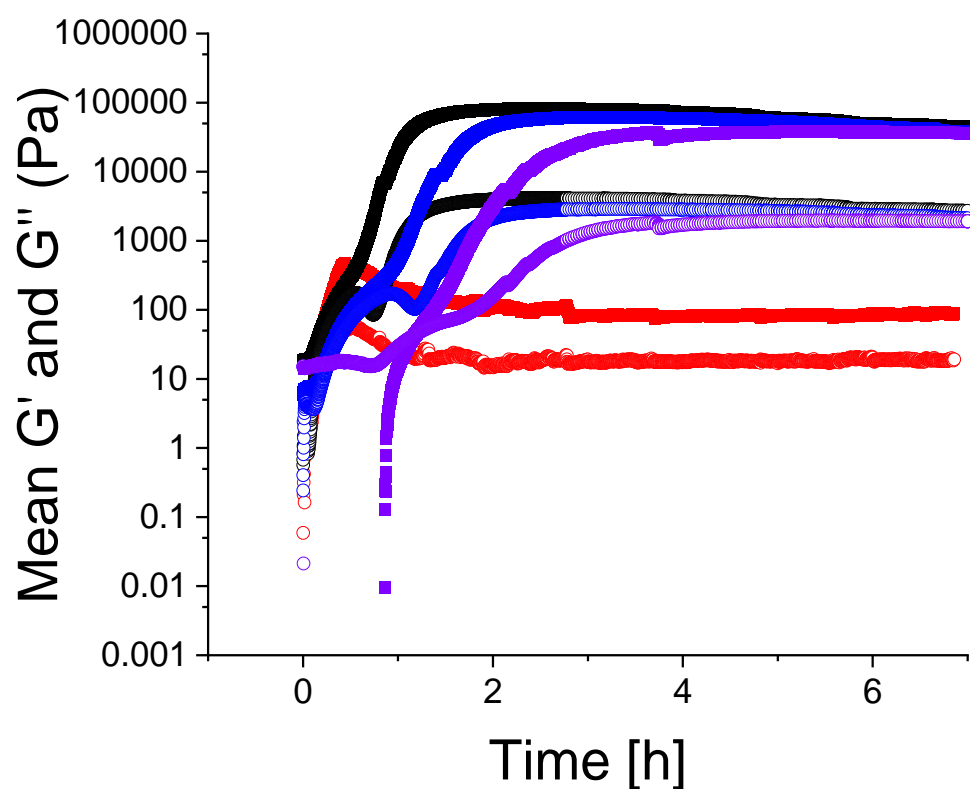
Figure S16: Rheology time sweeps at 25°C (red), 15°C (black), 10°C (blue) and 5°C (purple) showing the change in kinetics for the gel to crystal transition as the temperature is lowered.

References

1.　　Chen, L.; Revel, S.; Morris, K.; C. Serpell, L.; Adams, D. J., Effect of Molecular Structure on the Properties of Naphthalene−Dipeptide Hydrogelators. *Langmuir* **2010,** *26* (16), 13466-13471.

2.　　Draper, E. R.; Dietrich, B.; McAulay, K.; Brasnett, C.; Abdizadeh, H.; Patmanidis, I.; Marrink, S. J.; Su, H.; Cui, H.; Schweins, R.; Seddon, A.; Adams, D. J., Using Small-Angle Scattering and Contrast Matching to Understand Molecular Packing in Low Molecular Weight Gels. *Matter* **2020,** *2* (3), 764-778.

3.　　Houton, K. A.; Morris, K. L.; Chen, L.; Schmidtmann, M.; Jones, J. T. A.; Serpell, L. C.; Lloyd, G. O.; Adams, D. J., On Crystal versus Fiber Formation in Dipeptide Hydrogelator Systems. *Langmuir* **2012,** *28* (25), 9797-9806.

4. www.sasview/org/